Corresponding Author: Dr. Jesús García-Lafuente, PhD

Corresponding Author's Institution: Univ. of Málaga

First Author: Jesús García-Lafuente, PhD

Order of Authors: Jesús García-Lafuente, PhD; Guillermo Díaz del Río; Consuelo Sánchez Berrocal

Vertical structure and bottom-intensification of tidal currents off Northwestern Spain

Jesús García-Lafuente[1], Guillermo Díaz del Río[2] and Consuelo Sánchez Berrocal [3]

[1] Departament of Applied Physics, University of Malaga, Malaga, Spain

[2] Oceanographic laboratory of A Coruña, Instituto Español de Oceanografía, Spain.

[3] SEK University, Segovia, Spain

Corresponding author address:

Jesús García-Lafuente

ETSI Telecomunicación, Campus de Teatinos s/n,

Universidad de Málaga, 29071, Málaga SPAIN

glafuente@ctima.uma.es

Tel: +34 952132721. Fax: +34 952131450

Abstract

Current and temperature observations collected in two different positions and at four different depths in the Golfo Artabro, off the NW corner of the Iberian Peninsula, have been analysed in order to investigate some aspects of tides in this area. Tidal currents in the deepest stations are much greater than expected for a purely barotropic tide, a result that is even more outstanding if the bottom decay of the interior currents is allowed for. The near-bottom tidal enhancement is confirmed by the large tidal fluctuations of temperature at M2 frequency, equivalent to internal oscillations of some tens meters of amplitude. The phase of these oscillations suggests propagation of the internal tide parallel to the bathymetry gradient. The slope of the bottom profile is comparable to the slope of the internal rays and favours the generation of internal tides of considerable amplitude. The existence of areas of supercritical slope shoreward of the mooring lines is able to reflect seawards the energy of the incoming internal waves along trajectories nearly parallels to the sea floor, a mechanism that is put forward as the responsible for the considerable concentration of tidal energy in the bottom layer.

1.- INTRODUCTION

Internal tides are generated by the interaction of the barotropic tide with topography in the presence of stratification. The mechanism of generation involves the conversion of barotropic tide energy into energy of the internal motion and, in general, the efficiency of the conversion increases with stratification, topographic gradient and amplitude of the barotropic current (Baines, 1982). Large amplitude internal tides are observed to be efficiently generated around the continental shelf break and slope of many oceans and seas. They progress shoreward across the continental shelves where most of the internal tide energy is thought to be dissipated. But they also can radiate part of their energy back to the ocean either directly (New and Pingree, 1992) or after reflection in a supercritical topography (topographic slope greater than the slope of the internal beams). Frequently, the onshore propagating waves steepen through non-linearity and, eventually, may form internal bores that evolve in short-period wave packets to finally disappear by mixing (Holloway, 1987; Colosi et al., 2001).

In the eastern North Atlantic, the Armorican shelf in the northern Bay of Biscay (Pingree et al., 1986; New, 1988; Pingree and New, 1989) or the Malin shelf to the north of Ireland (Sherwin, 1988; Small et al., 1999; Rippeth and Inall, 2002) are well studied regions of internal wave generation. To our knowledge, detailed studies of the internal tide in the continental shelf and slope region off the north-west corner of the Iberian Peninsula (Figure 1) do not exist yet. Among the few references of tidal motions in this area are the observations collected by a vessel-mounted Acoustic Doppler Current Profiler (ADCP) at around 42ºN (Figure 1) by Barton et al. (2001). The data suggest the existence of a mode 1 internal tide on the continental shelf off Galicia with a top to bottom maximum vertical shear of about 0.15 m s^{-1}. Over the continental slope, the observed tidal shear was much reduced and the vertical structure more complicated. They also reported a phase lag of the eastward component of the ADCP velocity that increased toward the surface, indicating that the tidal energy was progressing upwards. They point out that the observations were compatible with an internal tide generated offshore and present a Synthetic Aperture Radar image showing the surface signature of high frequency internal waves propagating towards the shore. These internal wave packets appear to be phase-locked with the barotropic tide (Jeans and Sherwin, 2001) and they probably correspond to the non-linear evolution of the onshore progressing

3

internal tide, as reported in Colosi et al (2001). Huthnance et al. (2002) report predominantly semidiurnal currents of around 0.1 m·s^{-1} on the continental shelf off west Iberia that diminish to half this value in the open ocean. Deep water ellipses are along-slope but they gain an increased cross-slope component on the upper slope and outer shelf, specially close to the bottom. Vitorino et al. (2002) show an example of bottom-intensification in 41º 22'N at 1200 m depth in a bottom of 2300m, with tidal currents as large as 0.2 m s^{-1} inside of Porto submarine canyon.

During the "*Study of the coastal circulation*" Project, instruments deployed in the Golfo Artabro, to the north-west of A Coruña (Figura 1), measured tidal velocities as large as 0.2 ms^{-1} near the sea floor. The instruments were not inside any submarine canyon, where amplification of currents is not unusual (see García-Lafuente et al., 1999, for instance), making of this bottom-intensification an intriguing feature that has motivated this study. It has been organised as follows: Section 2 presents the data and Section 3 presents the results of the tidal analysis, which shows an intense baroclinic tide near the bottom. Section 4 discusses some aspects of the internal wave kinematics and analyses the results from the ray tracing approach. Section 5 summarises our conclusions.

2.- DATA

From May 15 to September 12, 1996, an array of two mooring lines with 4 currentmeters each was deployed in the Artabro Gulf, off the northwestern tip of the Iberian Peninsula (see Figure 1). The deployment was part of the program "*Study of the Coastal Circulation*" funded by the Instituto Español de Oceanografía (IEO). Two oceanographic surveys consisting of Conductivity-Temperature-Depth (CTD) casts were carried out at the beginning and at the end of the mooring deployments. The CTD stations during ARTABRO1 survey (May 1996) are shown in Figure 1. The present study focus on the observations collected by the currentmeter array and the CTD information has been used only marginally.

Instruments were moored at the nominal depths of 150m, 300m, 700m and 1100m in both sites (see Figure 1) in a bottom depth of 1170m (site A) and 1180m (site B). The common period of sampling started on May 15 at 15:00 GMT and finished on September 12 at 10:00, which provides a 120-day long time series of velocity and water

temperature with a sampling interval of 30 minutes. The depths of measurements have been numbered from top to bottom and are denoted by a unique code formed by a letter followed by a number: for instance, A3 indicates the station at depth 3 (700m) in position A and so on.

Other datasets utilised in the study have been sea level records of nearby Spanish ports, mainly A Coruña, downloaded from the IEO database. The data were used to carry out comparisons between the harmonic constants of sea level and velocity observations. Bottom topography from Sandwell and Smith bathymetry has been used in order to assess the importance of bottom slope on internal-tide generation and propagation.

3.- RESULTS

Harmonic constants of the observations have been computed following the method developped by Foreman (1978, 1996) and implemented by Pawlowicz in MATLAB (Pawlowicz et al, 2002). Two types of analysis have been performed, the vectorial version for velocity observations and the escalar analysis for sea level and temperature obeservations. The results for either of them are presented next.

3.1 Tidal currents
Tidal currents show prevalence of the semidiurnal species and, within this species, of M2 constituent, whose harmonic constants are presented in Table 1 for all stations. Figure 2 shows the same information graphically. The most noticeable result is the intensification of tidal currents in the deepest level (stations A4 and B4), which is accompained by the cross-bathymetry orientation of the tidal ellipses. Major semiaxis at this level is about twice the major semiaxis at any other depth and largely exceeds the expected value of the barotropic tidal current. This value could be roughly estimated using the theory of barotropic Kelvin waves propagating along an straight coastline, which predicts null cross-shore velocity and along-shore velocity in geostrophic balance with surface tide. At a distance x from the shoreline, the amplitude of the fluctuating alongshore velocity is given by (Gill, 1982)

$$v_0 = \eta_0 \sqrt{\frac{g}{H}} \, e^{-\frac{x}{a}} \qquad\qquad (1)$$

where η_0 is the amplitude of tidal elevation at the shore, g is gravity, H is the water depth and a is the external Rossby radius of deformation, $a=(gH)^{1/2}/f$. At 43°N, the Coriolis parameter f is 9.9 10^{-5} s^{-1} and $a \approx 1000$ km for H=1000m, a representative bottom depth at the location of mooring lines. Harmonic analysis of sea level records in A Coruña (Figure 1) gives 1.18 m and 86° for the amplitude and phase of M2 constituent, respectively. With these values equation (1) yields v_0 =11.1 cm s^{-1}, about half the major semiaxis of the tidal ellipses of stations A4 and B4. The shoreline is not straight in the sampled region but it turns abruptly to the east at almost right angle. Kelvin theory is not applicable; a more realistic pattern is the superposition of Kelvin and Poincare modes giving a more complex wave motion. Battisti and Clarke (1982) put forward a simple theory to compute barotropic tidal curents on a continental shelf in which the cross-shore and alonshore velocities are given by

$$u_0 = \frac{i\omega\eta_0 x}{H} \qquad\qquad (2)$$

$$v_0 = \eta_0\left(\frac{fx}{H} + \frac{g}{c}\right) \qquad\qquad (3)$$

where ω is the frequency of the tidal constituent, M2 in this case ($\omega_{M2} = 1.4 \ 10^{-4}$ s^{-1}) and c is the phase speed, given by $c=(gH)^{1/2}$. Using these equations, we obtain u_0=0.8cm s^{-1} and v_0=12.3cm s^{-1}, values that hardly differ from the previously computed u_0=0, v_0=11.1cm s^{-1} using the Kelvin wave dynamics. The tidal ellipse predicted by (2) and (3) is very eccentric, a result also found by Alvarez Fanjul et al. (1998) when computing tidal ellipses in the North Atlantic from a numerical model. Nevertheless, these theoretical values are arguable due to the oversimplification of the models.

An experimental barotropic tide can be estimated from the observations as a depth-averaged velocity. The scarce sampling of the water column makes it difficult to determine the weights by which the observations must be multiplied in the numerical integration. If they are proportional to the column thickness that a given station

represents, the weights would be [0.20, 0.24, 0.35, 0.21]. With these weights, the harmonic constants of depth-averaged velocity in position B are 4.2 cm s^{-1} and 3.4 cm s^{-1}, 144º and 172º for the major and minor semiaxis, inclination and phase, respectively while in A they are 8.6 cm s^{-1}, 1.0 cm s^{-1}, 36º and 58º for the same parameters. Taking into account the spatial scale of coherence of a barotropic wave, there is no physical reason for such large discrepancies between two locations separated only few kilometres. Values in A are close to the predictions of equations (2) and (3), although inclination is somewhat less than the orientation of the isolines of bathymetry (Figure 1). On the contrary, the orientation of the tidal ellipse in B is across the bathymetry, a non-surprising result in view of the intense tidal currents in station B4, which bias the depth-integrated velocity towards the values in this station. A cross-slope orientation is not compatible with the expected barotropic ellipses in this region, where the tidal wave progress northward parallel to the isolines of bathymetry.

Table 1 and Figure 2 show a tendency of harmonic constants in position A to increase from station A3 towards the surface. It suggests that the weight of the upper part of the water column is underestimated in the vertical mean. In this case a re-definition of the whole set of weights with a greater first weight would be reasonable in order to compensate for that underestimation. The increase is not so evident in position B. We have tried different possibilities, always with the first weight greater than any other. An additional constrain has been imposed in the sense that the resulting tidal ellipse must be oriented along the isobaths and the phase must be similar to the phase of sea level, as it has to be for a progressive wave. A Coruña has been the coastal station used for reference, therefore the phase of tidal ellipses should not much differ from 86º, the phase of sea level. After some trial-error runs, the set of weights [0.40, 0.20, 0.25, 0.15] have shown to fulfil satisfactorily both conditions (see rows in italics in Table 2). Notice, however, that the amplitude and the ellipse eccentricity in position B are much less than in A. In the last station the whole set of harmonic constants is now more compatible with predictions of equations (2) and (3) and, hence, with the progressive wave dynamics. The relative lack of agreement in B is surely due to the strong baroclinic nature of tides at level 4.

The baroclinic or internal contribution of M2 to the tide has been computed carrying out the harmonic analysis to the series obtained removing the depth-averaged velocity from

the observations at each station. Table 2 shows the harmonic constants derived from the analysis. All ellipses rotate clockwise, an expected feature of internal tides in the northern hemisphere, and the ratio of minor to major semiaxis (last column of Table 2) has tendency to be close to the ratio f/ω_{M2} (-0.706 at 43ºN, the minus sign indicating clockwise rotation), which is the theoretical value deduced from the linear theory of internal waves (Gill, 1982). The agreement is particularly good for the deepest stations A4 (-0.67±0.03) and B4 (-0.70±0.02), the two stations of largest internal M2 signal. It is worth noting that the internal tide ellipses of other semidiurnal constituents (S2, N2) deduced through this barotropic/baroclinic decomposition also show minor to major axis ratio agreeing very well with theory (ratios of -0.63±0.06 and -0.72±0.06 for S2 in A4 and B4, respectively, against the theoretical value of -0.683 at 43ºN and -0.64±0.10 and -0.67±0.11 for N2 in A4 and B4, against the theoretical value of -0.719). We want to mention these results as an *a posteriori* justification of the empirical procedure followed to compute the barotropic, depth-averaged velocity. It is also worth noting the clear cross-slope orientation of the baroclinic ellipses in A4 and, specially, in B4.

3.2 Internal oscillations

Temperature records show tidal fluctuations of semidiurnal frequency in all stations (Figure 4). Columns 2 and 3 of Table 3 show the amplitude and phase of these fluctuations at M2 frequency, while column 4 is the percent variance explained by tides. The largest amplitude is found in station B4 where tidal oscillations explain more than 62% of the variance. Station A4 exhibits a similar pattern. On the contrary, the lowest amplitudes and explained variances are found in stations A3 and B3. Stations in level 1 have relatively large amplitude but tides hardly explain 25% to 30% of the variance, indicating that they are not the main source of variability. At level 4, however, they are.

Vertical velocity can be computed from temperature oscillations according to

$$w = -\frac{\partial T / \partial t}{\partial T / \partial z} \tag{4}$$

which comes from the equation of conservation of thermal energy if heat diffusion and horizontal advection of temperature are ignored. At tidal frequencies in a region without important horizontal temperature gradients both approximations are reasonable. The

numerator of equation (4) is readily obtained from the temperature time series, but the denominator is not well determined from the poor-vertical-resolution of the mooring array.

Representative profiles of temperature nearby positions A and B in May and September are available from the CTD surveys and are plotted in Figure 5. The profiles have spatial and temporal variability that complicates the estimation of reliable vertical gradients of temperature. However, even when the temperature profile changes nearby levels 1, 2 and 4, the variability hardly affects the vertical gradient of temperature, a fact that is specially true in levels 2 and 4. On the contrary, the variability strongly affects the gradient of temperature in level 3, to the point that even the sign of $\partial T/\partial z$ cannot be well defined (Table 3). Figure 5 shows that stations A3 and B3 are situated above the Mediterranean core near the local minimum of temperature, where $\partial T/\partial z=0$. Both stations have warmer water beneath, which raises the possibility of having $\partial T/\partial z$ negative (increase of temperature with depth, a situation unusual in the real ocean), but the gradient can be also positive if the Mediterranean water sinks. Therefore, vertical displacements of the Mediterranean flow may change the sign of $\partial T/\partial z$ at this level, implying a null value of the gradient as the temperature minimum passes through the station. Whenever this happens, the time derivative $\partial T/\partial t$ must be null too in order to keep w finite in equation (4). An example of this situation is shown in the left panel of Figure 4: around yearday 180, the temperature in A3 does not fluctuate. A detailed inspection indicates that, previously to that date, the slowly-varying temperature was above 11ºC to decrease to less than 11ºC after day 182. A quite probable scenario is the station being initially in the upper part of the Mediterranean core, which progressively sunk leaving the instrument in colder water after day 182. In doing so, the temperature minimum had to pass through station A3 forcing the time derivative to be null during the transition. The absence of temperature fluctuations between days 176 and 182 along with the fact that temperature was fluctuating out of phase in A3 and A4 before day 175 and almost in-phase after day 182 support this interpretation. The fact that tidal variance at level 3 is by far lesser than at any other level (Table 3) is quite probably related to the nearness of this level to the temperature minimum. While interesting, this curious behaviour is a drawback for using equation (4) to estimate w. Therefore, the vertical

9

velocity computed at stations A3 and B3 from this equation must be considered cautiously, particularly in A3.

Column 5 of Table 3 shows the vertical gradients of temperature computed from the temperature profiles collected during the surveys of May and September. The bottom panel of Figure 5 shows that the gradient in level 1 is stronger in September due to the development of the seasonal thermocline, but it remains essentially unaltered in levels 2 and 4. According to the previous discussion, the temperature gradients at stations A3 and B3 are rather uncertain, even regarding its sign. In A3, the gradient is positive in May and negative in September (Table 3). The fact that temperature phase in A3 is similar to phases in A1 and A2, where the vertical gradient of temperature is clearly positive, would justify a positive value for $\partial T/\partial z$ in this station. This would lead to a vertical velocity in A3 comparable to w in A2 and A1. But a negative temperature gradient would bring the phase of w in A3 close to the phase in A4, which would is physically reasonable too. Thus the uncertainty of $\partial T/\partial z$ in A3 makes us to discard this station. On the contrary, the almost 180º out-of-phase of temperature signal in B3 with regards to the phase of the three other stations in position B suggests that the sign of $\partial T/\partial z$ must be negative and, in fact, it has this sign during both surveys.

The harmonic constants of the vertical velocity can be computed using the harmonic constants of temperature in Table 3 according to

$$W_{M2}(z) = \frac{\omega_{M2} B_{M2}(z)}{(\partial T/\partial z)} \qquad (5.a)$$

$$\phi'_{M2}(z) = \phi_{M2}(z) - \frac{\pi}{2} \qquad (5.b)$$

where $W_{M2}(z)$ and $\phi'_{M2}(z)$ are the amplitude and phase of the vertical velocity at level z and $B_{M2}(z)$ and $\phi_{M2}(z)$ the amplitude and phase of the temperature signal. If equation (5.a) gives $W_{M2}(z)$ negative, which happens in B3 and maybe in A3, the minus sign is passed to the phase by adding 180º. Alternately, the harmonic constants of w can be

estimated computing the time derivative of T, dividing this series by $\partial T/\partial z$ and performing harmonic analysis on the resulting series. Both methods give almost identical harmonic constants. Columns 6 and 7 of Table 3 show the constants estimated through the first approach. The associated errors do not include the uncertainty in $\partial T/\partial z$, which cannot be estimated from our dataset. An error double than the reported one is surely more realistic. A simple integration of w provides the harmonic constants for the internal oscillations, which are listed in the two last columns of Table 3.

The internal oscillations so computed indicate that the greatest vertical velocity and internal amplitude are achieved in level 4, in good agreement with the analysis of the horizontal velocity field. The baroclinic tide tends to concentrate energy in the bottom layer. In position B, the phase of internal oscillations has clear tendency to increase with depth (Figure 5), which implies downwards propagation of phase and therefore upwards propagation of the internal energy.

4.- INTERNAL WAVE KINEMATICS

Within the WKB approximation of internal waves, the vertical wavenumber m of the internal M2 tide can be computed

$$m = \frac{\partial \phi_{M2}(z)}{\partial z} \tag{6}$$

where ϕ_{M2} is either the phase of the internal oscillations or of the vertical velocity (they differ by $\pi/2$ radians, which does not affect the z-derivative). A first estimation of m as the slope of the straight line in Figure 5 gives $m=-6.7 \ 10^{-4} \ \text{m}^{-1}$ in position B. The lack of information about the phase in station A3 prevents us from carrying out a similar estimation in position A. According to the linear theory of waves, the characteristic (the path of internal energy beams) of the waves is given by (Gill, 1982)

$$\tan \alpha = \pm \sqrt{\frac{\omega_{M2}^2 - f^2}{N^2 - \omega_{M2}^2}} \tag{7}$$

where N is the buoyancy frequency and α is the angle the characteristic forms with the horizontal plane. The sign of the right hand side is opposite to the sign of m in order to verify the classical result of energy and phase progressing in different directions along the z-axis. If $\boldsymbol{k}=(\boldsymbol{k_H}, m)$ is the wavenumber vector ($\boldsymbol{k_H}$ the horizontal wavenumber) the energy will travel along the line parallel to $(-m, \boldsymbol{k_H})$ and therefore $\tan\alpha =-k_H/m$. This relationship along with equation (7) determines the magnitude of $\boldsymbol{k_H}$

$$k_H = m\sqrt{\frac{\omega_{M2}^2 - f^2}{N^2 - \omega_{M2}^2}} \qquad (8)$$

Equations (6) and (7) are applicable in the ocean interior where the buoyancy frequency is nearly constant or, at least, a slowly-varying function of z.

The analysis of the two types of data carried out in section 3 has shown that the deepest stations A4 and B4 have the greatest internal tide. Even more, the variance of currents in A4 and B4 is the largest of all stations and more than 80% of this variance is accounted for by tides; current variability is basically tidal motions and tides are mainly baroclinic judging from the results shown in Figures 2 and 3. The analysis of temperature records provides similar conclusions. Therefore, we focus the following analysis on the data collected in these two deep stations.

4.1.- Internal tide in the bottom layer
The phase of the vertical oscillation in station B4 leads the phase of A4 by 19º (Table 3), suggesting that the internal tide propagates from B to A. From phase values alone, it is not possible to determine the direction of propagation of the tide; the most we can say is that internal tide reaches position B around 40 minutes (equivalent to 19º for M2 frequency) earlier than in position A. Additional information, however, can be drawn from equations (7) and (8). The buoyancy frequency at the depth level of stations A4 and B4 computed from the CTD data ranges from 2.1 10^{-3} s^{-1} to 2.4 10^{-3} s^{-1}, with a slight bias toward the upper limit. These values in turn give beam slopes between 0.047 and 0.041 from equation (7), horizontal wavenumbers between 3.15 10^{-5} m^{-1} and 2.72 10^{-5} m^{-1} from equation (8) and horizontal wavelengths of 200 km and 230 km, respectively.

The representative horizontal wavelength we will work with is 220 km, slightly biased towards the upper limit, which corresponds to a horizontal wavenumber k_H =2.86 10^{-5} m^{-1}.

Assuming plane internal waves, the phase difference between positions A and B is given by the dot product $k_H \cdot r_{A-B}$, where r_{A-B} is the vector that starts in B and ends in A (see sketch of Figure 7) whose magnitude is 30 km, the distance separating both sites. The dot product depends on the relative orientation of vectors k_H and r_{A-B}. If they were parallel, the phase difference given by the dot product would be 49º, much greater than the observed 19º. Even more, it would be clearly outside the error interval (±9º) of the estimation. Therefore r_{A-B} cannot be the direction of propagation of a plane wave baroclinic tide.

The direction of k_H for which the dot product is 19º is straightforwardly computed: for k_H =2.86 10^{-5} m^{-1}, it is 136º from the east, and ranges from 125º to 150º if the error of the phase difference is taken into account. This direction is perpendicular to the topography of the continental slope (Figure 7), which is an encouraging result as this is the preferred direction for propagation of the internal tide if it is generated at the continental slope (Rattray et al., 1969; Baines, 1982). Figure 3 shows that this direction roughly coincides with the orientation of the baroclinic tidal ellipses, a fact that support our analysis. Therefore one could think of the baroclinic tide as being generated shorewards of positions A and B and progressing seawards from there passing through station B4 first and then through station A4. This hypothesis is analysed in next Section. To conclude this one, the baroclinic part of the velocity field in stations A4 and B4 has been decomposed into parallel and normal-to-topography components and the last one has been analysed to find their harmonic constants. The reason to carry out this analysis is to check whether or not the phase difference of the offshore component in both stations supports the results found for the vertical displacements. The baroclinic velocity has been projected in a Cartesian system rotated +136º anticlockwise so that the new *x*-component of the velocity points offshore in the direction of the gradient of the local topography. The amplitudes and phases of M2 in A4 and B4 are 15.5±1.1 cm s^{-1}, 223±4º and 17.7±1.0 cm s^{-1}, 199±3º, respectively. Station B4 leads station A4 by 24º, in quite good agreement with the 19º lag of vertical oscillations. However the

relative values of the phases of velocity and vertical oscillation at a given station are not compatible with the theory of progressive waves, which demands the same numerical value for both variables.

4.2 A possible mechanism of near-bottom intensification of the internal tide.

The continental slope off Galicia is very step (Figure 7) and propitious for the generation of internal tides. Figure 8a shows the bottom topography along the transect depicted by the dashed thick line in Figure 7, the origin of the *x*-axis being point "O". Vertical lines labelled A and B are indicative of the relative positions of moorings A and B and the topography of the continental slope along the transect (actually, the lines are obtained projecting positions A and B perpendicular to the transect). According to the discussion in the previous section, this transect would be a preferred direction for the propagation of a plane internal tidal wave, reason for which it has been selected for the following analysis. Figure 8b shows the bottom slope and the characteristic of the internal M2 internal wave nearby the bottom. The buoyancy frequency necessary to compute the ray slopes from equation (7) has been obtained from the CTD dataset. In particular, we have used the offshore transect containing CTD stations 22, 23 and 24 (Figure 1). The vertical profiles of *N* beyond the outermost station (station 24) are assumed to coincide with the vertical profile of this station until the depth of the deepest observation and constant from there to the bottom. It is a crude approximation that leads to the constant slope of the rays in the deeper part of the transect (horizontal lines in Figure 8b) but otherwise does not have consequences for tracing the internal wave rays nearby the locations of the moored lines.

Figure 8b shows that in the neighbourhood of the hypothetical situation of the moorings, the continental slope is close to critical over a large area, which implies an efficient generation of internal tides (New, 1988; Balmforth et al., 2002). Furthermore, the continental slope becomes supercritical shoreward of position B. The internal tide eventually generated in the critical area and progressing to the shore will be reflected back to the ocean in the supercritical region. The situation is illustrated in Figure 8c, which shows an enlarged area of the vertical profile shown in Figure 8a. There are two possibilities for such reflection: the first one is rays emanating upwards (grey lines), while the second possibility corresponds to rays pointing downwards (black lines).

These reflected rays tend to concentrate energy in the bottom layer as they run almost parallel to the bottom topography, which has approximately the same slope since the bottom is nearly critical. They would be responsible for the increased tidal energy registered at the near-bottom stations.

Eventually, the down-propagating rays would be reflected upwards once they go out the supercritical zone (highlighted with the thick grey line in Figure 8c), giving rise to places where most of internal beams propagate upwards. The precise location of these places would be function of their distance to the zone of supercritical continental slope. Figure 8c suggests that mooring line B could have been located in one of these places, which would explain the regular increasing of phase with depth shown in Figure 6. If the mooring line were further apart from the supercritical region, the spatial pattern of the beams crossing the position would be less regular and not to leave a clear signature. Mooring A could have been situated in such a distance and, hence, the irregular behaviour of phase observed in this position.

4.3 Intermittency and spatial coherence of the internal tide.

The very simple approach of the previous Section shows that wave kinematics is capable of explaining some of the observed features of the internal tide. We realise however that the conclusions drawn from this approach are very arguable. To start with, Figure 8c does not pretend to accurately represent the internal wave beams because the ray trajectories are sensitive to the bottom topography and to the stratification. Slight changes of any of these ingredients may change noticeably the sketched beams. Therefore, it is rather coincidental that projections of positions A and B on the selected normal-to-topography transect lay on the right place to meet the requirements needed for explaining the dependence of phase with depth. But the ray tracing method has shown that the possibility exists. The important thing for this method to explain the enhanced tidal energy in the near-bottom layer is that the continental slope reaches supercritical values shoreward of the mooring lines in order to allow for backwards reflection of the internal tide.

The second important drawback is the well-known intermittent nature of the internal tide and its rather reduced spatial scale of coherence. The kinematics approach has

assumed implicitly that the M2 internal oscillations have rather constant values of amplitude and phases, which in turn implies that the internal tide is coherent with the barotropic tide over long periods of time. Although coherence over periods of time of the order of a spring-neap tidal cycle has been reported (Sherwin, 1988), the usual situation is not to find a phase-locked relationship between baroclinic internal tide modes and the barotropic tide (Wunsch, 1975).

To get more insights on the temporal and spatial scales of coherence, the time series of temperature and velocity in stations A4 and B4 have been split in pieces 20-day long and subjected to harmonic analysis. The harmonic constants of the different pieces are shown in Figures 9a and 9b for temperature and in Figures 10a to 10d for velocity. All these Figures make the intermittency of the baroclinic tide clear but they also show some properties that remains reasonably unaltered with time. This is the case in station B4 where the different harmonic constants show a rather regular behaviour with time. It suggests that the station is under the influence of a generation or amplification mechanism phase-locked with the barotropic tide. Such mechanism could be the local generation of the internal tide in the nearby supercritical continental slope and its offshore radiation along beams running parallel to the bottom, as discussed in Section 4.2.

Another interesting feature is provided by the analysis of the spatial correlation in Figure 9C. This Figure shows contours of the correlation coefficient between temperature series in A4 and B4 computed for 7-day long and for different time lags. The maximum correlation is regularly obtained for phase lag between −1 and 0 hours, A4 lagging B4, in good agreement with the average 19º provided by the harmonic analysis. The correlation for these lags is greater than 0.6 except for short periods around days 160 and 200 when a notable attenuation of the signal is observed in A4. The reasonably good correlation indicates that the spatial-scale of coherence of the baroclinic tide exceeds the distance between stations A4 and B4, a fact that is further confirmed by Figure 10D, which shows the same pattern for phases at both stations. This curious similarity contrasts with the fluctuating and even chaotic temporal pattern, which suggests a pronounced intermittency in time but a consistent spatial coherence.

5.- CONCLUSIONS

The current and temperature observations collected in two different positions and at four different depths in the Golfo Artabro, off the NW corner of the Iberian Peninsula, have been analysed in order to investigate some aspects of tides in the area. Tidal currents in the deepest stations are much greater than expected for a purely barotropic tide, a result that is even more outstanding if the bottom decay of the interior currents is allowed for. To further investigate this feature, velocity observations have been separated out in a depth-independent barotropic and a baroclinic components, the harmonic constants of the former being similar to those expected for a barotropic progressive wave. The baroclinic part of the velocity field shows great amplitude at the deepest stations, and much less amplitude at the others. The near-bottom tidal intensification is confirmed by the noticeable and regular tidal fluctuations of temperature at M2 frequency, which are equivalent to internal oscillations of some tens meters of amplitude. Moreover, the orientation of the tidal ellipses is clearly in the cross-slope direction, a typical feature of baroclinic tides when they are generated in the continental slope.

On average, internal oscillations in station B4 leads oscillations in A4 by 19º, which suggests propagation of the internal tide from position B to position A, an hypothesis supported by the fact that tidal currents and internal oscillations in B are greater than in A. In position B the phase of internal oscillations increases steadily with z and this regular behaviour has been used to estimate a vertical wavenumber of $m=-6.7 \ 10^{-4} \ m^{-1}$ and a horizontal wavenumber $k_H =2.86 \ 10^{-5} \ m^{-1}$ (horizontal wavelength of around 200 km) from the equation of the characteristics. For a simple model of plane waves, the direction for which the phase difference between A and B is 19º is given by the dot product $r_{AB} \cdot k_H$, which is readily computed to be 135º. This is the orientation of the topography gradient, which is the preferred direction for propagation of internal tides generated at the continental slope. For this reason, we have analysed the bottom profile comparing its slope with the slope of the internal rays to conclude that the continental slope off NW Spain has many areas of near-critical slope that favour the generation of internal tides of considerable amplitude.

More important is the existence of areas of supercritical slope shoreward of the mooring lines where internal rays are reflected back to the ocean and downwards, following

trajectories nearly parallels to the sea floor. Downward propagation of internal tidal energy in the Biscay Bay has also been described by Pingree and New (1989). This is the mechanism we put forward here to explain the considerable concentration of tidal energy in the bottom layer. The mechanism is likely to exist everywhere along the upper part of the continental slope, near the continental shelf break where the slope is step. If so, the reflected waves radiated from different regions would interfere giving rise to a complicated wave pattern and a phase relationship between stations with important random contribution. However, an analysis of correlation shows that the tidal signals are coherent over distances greater than the distance separating positions A and B and the difference of phases tends to be stable.

A detailed inspection of the bottom topography (Figure 7) shows a very steep, supercritical area near position B, which could play the role of energy source for internal tides, thus explaining the greater amplitude observed in station B4 and the apparent propagation from B to A. Also, it would help explain the more regular spatial (in the vertical) and temporal behaviour of tides in B. The results of the ray tracing technique support this conclusion. On the contrary, although stations in position A are still under the influence of this somewhat remote source here, they are also exposed to other local (and probably less efficient) sources, thus giving rise to a more complex vertical and temporal pattern.

References

Alvarez Fanjul, E., Pérez, B. and Rodríguez, I., 1997. A description of the tides in the Eastern North Atlantic. Prog. Oceanog., 40, 217-244.

Baines, P.G., 1982. On internal tide generation models. Deep Sea Res., 29, 307-338.

Balmforth, N.J., Ierley, G.R. and Young, W.R., 2002. Tidal conversion by nearly critical topography. J. Phys. Oceanogr., 32, 2900-2914.

Barton, E.D., Inall, M.E., Sherwin T.J. and Torres, R. 2001. Vertical structure, turbulent mixing and fluxes during Lagrangian observations of an upwelling filament system off Northwest Iberia. Prog. Oceanog., 51, 249-267.

Battisti, D.S. and Clarke A.J., 1982. A simple method for estimating barotropic tidal currents on continental margins with specific application to the M2 tide off the Atlantic and Pacific coast of the United States. J. Geophys. Res., 12, 8-16.

Colosi, J.A., Beardsley, R.C., Lynch, J.F., Gawarkiewicz, G., Chiu, C.S. and Scotti, R., 2001. Observations of nonlinear internal waves on the outer New England continental shelf during the summer Shelfbreak Primer study. J. Geophys. Res., 106, 9587-9601.

Foreman, M.G.G., 1978: Manual for tidal currents analysis and prediction. Pacific Marine Science Repport 78-6. Institute of Ocean Sciences, Patricia Bay, Sidney, B.C., 57 pp.

Foreman, M.G.G., 1996: Manual for tidal currents analysis and prediction. Revised edition. Pacific Marine Science Repport 78-6. Institute of Ocean Sciences, Patricia Bay, Sidney, B.C., 57 pp.

García Lafuente, J., Sarhan, T., Vargas, M., Vargas, J.M. and Plaza, F., 1999. Tidal motions and tidally induced fluxes through La Línea submarine canyon, Western Alboran Sea. J. Geophys. Res., 104, 3109-3119.

Gill, A., 1982. Atmosphere-Ocean dynamics. Academic Press, New York, 662 pp.

Holloway, P.E., 1987. Internal hydraulic jumps and solitons at a shelf-break region on the Australian North-West shelf. J. Geophis. Res., 92, 5405-5416.

Huthnance, J.M., Van Aken, H. M. , White, M., Barton, E.D., Le Cann, B., Coelho, E. F., Alvarez Fanjul, E., Miller, P. and Vitorino, J., 2002. Ocean margin exchange-water flux estimates, J. Mar. Sys., 32, 107-137.

Jeans, D.R.G. and Sherwin, T.J., 2001. The evolution and energetics of large amplitude nonlinear internal waves on the Portuguese shelf. J. Mar. Res., 59, 327-353.

Levine, M.D. and Richman, J.G., 1989. Extracting the internal tide from data:Methods and observations from the Mixed Layer Dynamic Experiment. J. Geophys. Res., 94, 8125-8134.

New, A.L. 1988. Internal tidal mixing in Bay of Biscay. Deep Sea Res., 35, 691-709.

New, A.L. and Pingree, R.D., 1992. Local generation of internal soliton packets in the central Bay of Biscay. Deep Sea Res., 39, 1521-1534.

Pawlowicz, R., Beardsley, B. and Lentz, S. 2002. Classical Tidal Harmonic Analysis including Error Estimates in MATLAB using T_TIDE. Computers and Geosciences, 28, 8, 929-937.

Pingre, R.D., Mardell, G.T. and New, A.L., 1986. Propagation of internal tides from the upper slopes of the Bay of Biscay, Nature, 321, 154-158.

Pingree, R.D. and New, A.L., 1989. Downward propagation of internal wave energy in the Bay of Biscay. Deep Sea Res., Part A, 36, 735-758.

Rattray, M. Jr., Dworsky, J. and Kovala, P., 1969. Generation of long internal waves at the continental slope. Deep Sea Res., 16, 179-195.

Rippeth, T.P. and Inall, M.E., 2002. Observations of the internal tide and associated mixing across the Malin Shelf. J. Geophys. Res., 107, C4, doi 10.1029/2000JC000761.

Sherwin, T.J., 1988. Analysis of an internal tide observed on the Malin Shelf, north of Ireland. J. Phys. Oceanogr., 18, 1035-1050.

Small, J., Hallock, Z., Pavey, G. and Scott, J., 1999. Observations of large amplitude internal waves at the Malin Shelf edge during SESAME 1995. Cont. Shelf Res., 19, 1389-1436.

Vitorino, J., Oliveira, A., Jouanneau, J.M. and Drago, T., 2002. Winter dynamics on the northern Portuguese shelf. Part 1: Physical processes. Prog. Oceanog. 52, 129-153.

Wunsch, C., 1975. Internal tides in the ocean. Rev. Geophys. Space Phys., 13, 167-182.

Table 1.- Harmonic constants for M2 constituent in the sampled sites and at the different depths. Last column is the signal-to-noise ratio.

Station	Major semi-axis (cm/s)	Minor semi-axis (cm/s)	Inclination (degrees)	Phase (degrees)	S/N
Site A					
A1	13.9 ± 1.2	-7.0 ± 1.2	56 ± 7	94 ± 7	140
A2	10.0 ± 0.8	-5.0 ± 0.8	55 ± 6	86 ± 6	140
A3	6.9 ± 1.0	4.6 ± 1.3	2 ± 22	19 ± 19	48
A4	20.5 ± 1.1	-6.3 ± 1.2	5 ± 4	26 ± 3	380
Site B					
B1	7.4 ± 0.8	-1.5 ± 0.9	68 ± 7	80 ± 6	79
B2	8.0 ± 0.5	-0.8 ± 0.5	66 ± 3	90 ± 3	290
B3	6.4 ± 0.8	1.6 ± 0.7	66 ± 7	85 ± 7	65
B4	19.4 ± 0.9	-9.3 ± 0.9	-42 ± 3	12 ± 3	510

Table 2.- Harmonic constants for M2 frequency in sites A and B. Rows in italics show the constants of the depth-averaged velocity. The other rows show the constants of the baroclinic component of M2 computed as the difference between the original and the depth-averaged series. Column S/N is the signal-to-noise ratio. Last column is the ratio of minor (Sm) and major (SM) axis of the ellipse. Negative sign indicates clockwise rotation.

Station	Major semiaxis (cm/s)	Minor semiaxis (cm/s)	Inclination (°)	Phase (°)	S/N	Sm/SM
Site A						
Barotr.	*9.8 ±0.8*	*-1.3 ±0.8*	*50 ±4*	*77 ±4*	*350*	
A1	6.9 ± 0.6	-4.7 ± 0.6	182 ± 11	-10 ± 11	130	-0.69 ± 0.02
A2	4.3 ± 0.9	-0.9 ± 0.8	167 ± 11	9 ± 12	25	-0.21 ± 0.16
A3	7.8 ± 1.0	-4.1 ± 1.2	163 ± 13	154 ± 12	62	-0.53 ± 0.08
A4	17.9 ± 1.0	-12.1 ± 1.1	179 ± 7	191 ± 7	350	-0.67 ± 0.03
Línea B						
Barotr.	*4.7 ±0.5*	*2.4 ±0.5*	*63 ± 8*	*87 ± 8*	*94*	
B1	4.1 ± 0.5	-2.4 ± 0.6	127 ± 11	19 ± 11	82	-0.58 ± 0.05
B2	3.3 ± 0.5	-3.1 ± 0.5	76 ± 85	82 ± 85	38	-0.94 ± 0.01
B3	1.8 ± 0.7	-0.8 ± 0.7	82 ± 24	70 ± 26	6	-0.45 ± 0.21
B4	18.2 ± 0.8	-12.8 ± 0.9	118 ± 7	212 ± 6	470	-0.70 ± 0.02

Table 3.- Columns 2 and 3 in the first block (*T*) show the harmonic constants of temperature for M2 constituent. Column 4 is the percent variance explained by tidal oscillations. Column 5 is the local vertical gradient of temperature computed from the temperature profiles shown in the bottom panel of Figure 5. They are the mean of the values found at each station during surveys ARTABRO 1 and 2 (May and September) except for station A3, where the gradient was positive in May, negative in September and the mean nearly zero. It was the only station where the temperature gradient changed sign from one survey to the other. Block "*w*" shows the harmonic constants of the vertical velocity and block "*h*" presents the harmonic constants of internal oscillations. See text for details.

Sta-tion	M2: *T* Amp. (ºC)	Phase (º)	%	$\partial T/\partial z$ (ºC·m^{-1})	M2: *w* Amp. (mm/s)	Phase (º)	M2: *h* Amp. (m)	Phase (º)
Site A								
A1	0.20±0.02	43± 7	29.7%	6.5·10^{-3}	4.4 ± 0.6	313 ± 7	30 ± 3	223 ± 7
A2	0.13±0.02	93± 7	47.1%	4.4·10^{-3}	4.0 ± 0.5	3 ± 7	29 ± 5	273 ± 7
A3 [1]	*0.08±0.02*	*87±13*	*12.7%*	*3.4·10^{-3}*	*3.0 ±1.0*	*357±13*	*23 ±9*	*267 ±13*
A3 [2]	*0.08±0.02*	*87±13*	*12.7%*	*-3.5·10^{-3}*	*2.9 ±1.2*	*177±13*	*22 ±9*	*87 ±13*
A4	0.18±0.03	306± 8	40.1%	4.0·10^{-3}	6.1 ± 0.9	215 ± 8	45 ± 8	126 ± 8
Site B								
B1	0.23±0.03	255± 7	24.4%	6.0·10^{-3}	5.3 ± 0.6	165 ± 6	38 ± 5	75 ± 7
B2	0.05±0.01	250± 9	17.6%	3.6·10^{-3}	1.8 ± 0.3	160 ± 9	14 ± 3	70 ± 9
B3	0.08±0.02	92±11	10.7%	-2.3·10^{-3}	4.5 ± 1.2	182±11	34 ±12	92 ± 11
B4	0.27±0.03	287± 5	62.3%	4.6·10^{-3}	8.2 ± 0.7	197 ± 5	58 ± 7	107 ± 5

[1] Vertical velocity and amplitude of internal oscillations computed using the temperature gradient of May.
[2] Vertical velocity and amplitude of internal oscillations computed using the temperature gradient of September.
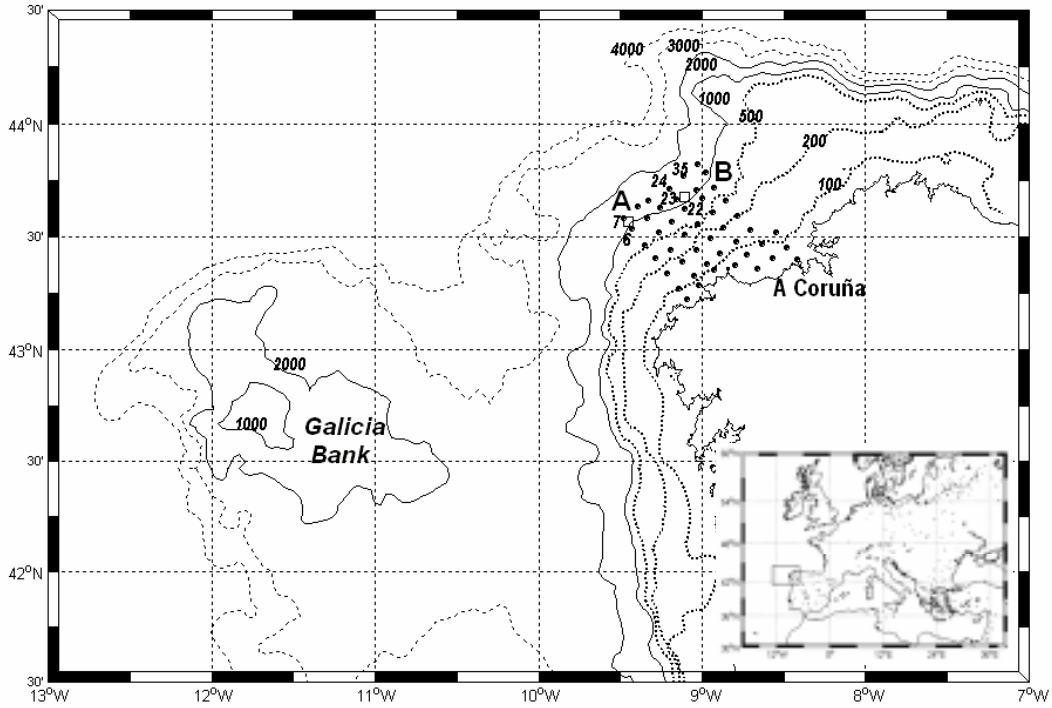
Figure 1.- Map of the area showing the bathymetry and the position of the mooring lines (empty rectangles, positions A and B). Dots indicate the location of the CTD casts accomplished during hydrographical surveys ARTABRO1 and ARTABRO2. CTD stations 6 and 7, nearby position A, and 22, 23, 24 and 35, around position B, have been labelled, since they are mentioned in the text. The remarkable bottom topography of the Galicia Bank has been indicated. The insert in the lower right part helps situate the area of study.
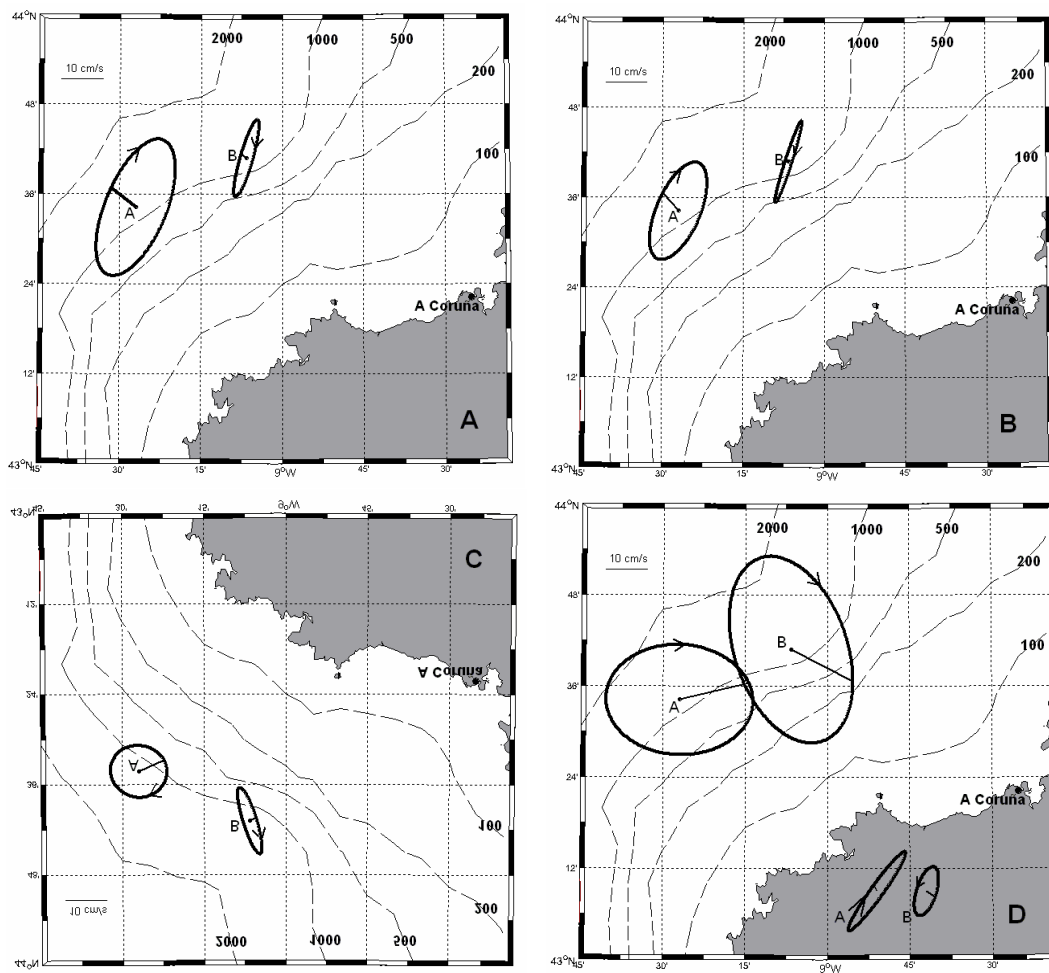
Figure 2.- Tidal ellipses of M2 constituent at the four sampled depths: Panels A, B, C and D are for depths 150m, 300m, 700m and 1100m, respectively. The velocity scale is on the top left corner of panels. The sense of rotation (clockwise except for depth #3) and the phase have been also indicated.
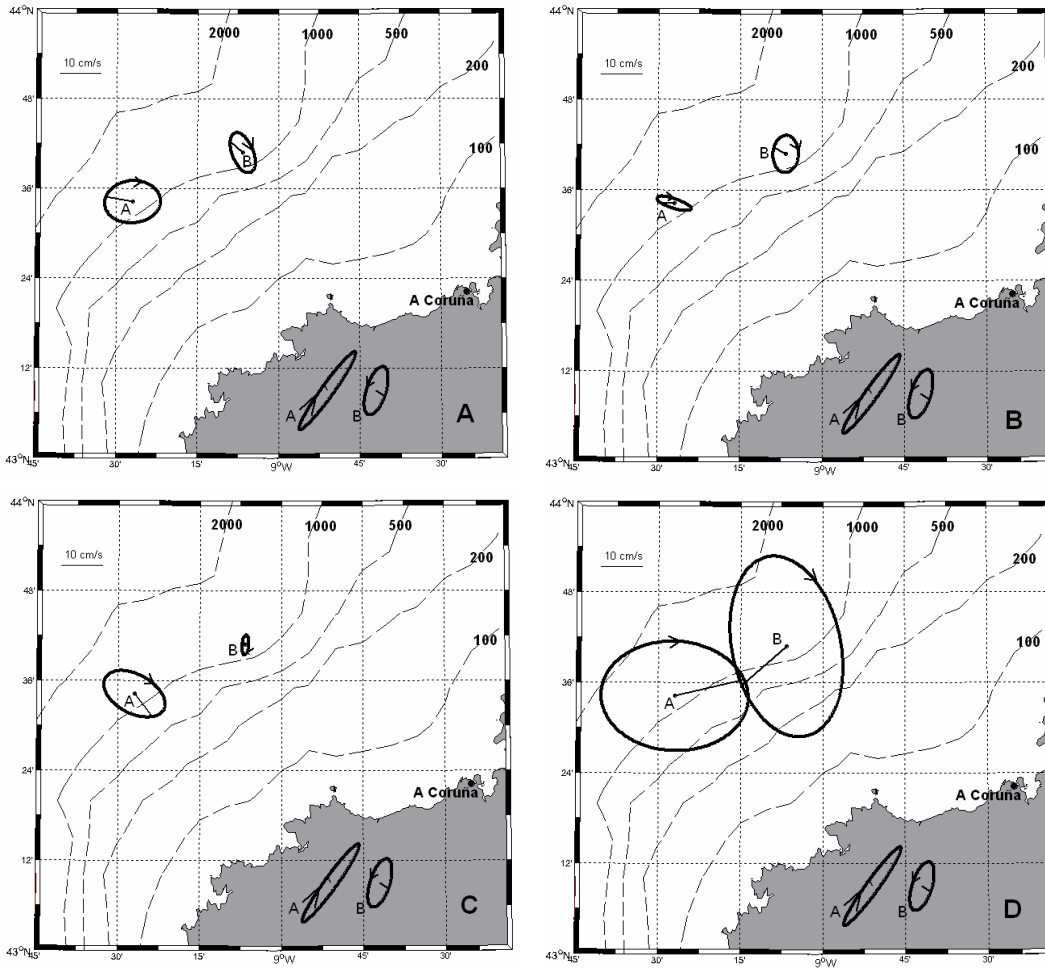
Figure 3.- Baroclinic tidal ellipses of M2 constituent at the four sampled depths: Panels A, B, C and D are for depths 150m, 300m, 700m and 1100m, respectively. The velocity scale is on the top left corner of panels. The sense of rotation (clockwise in all cases) and the phase have been also indicated. Tidal ellipses in the land-side of the map represents the z-independent barotropic component of the current in both positions (barotropic component, see text for details)
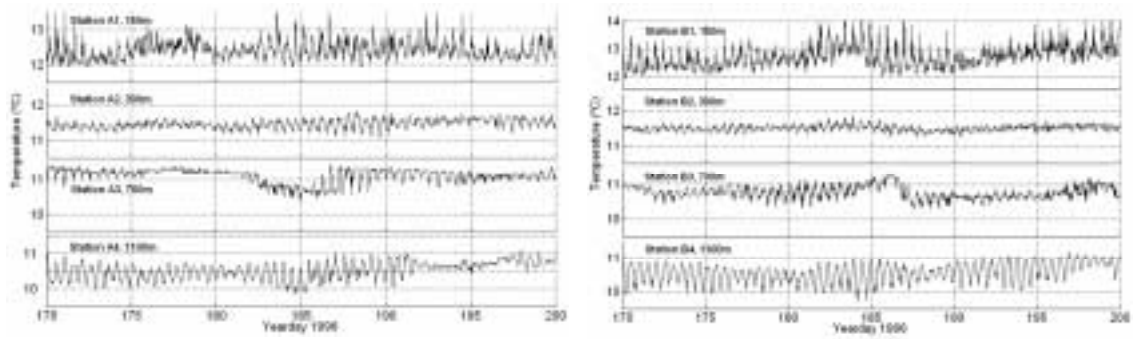
Figure 4.- Temperature time series at position A (left panels) and B (right panels) during part of the period of observations. More regular and distinguishable oscillations are recorded in the deepest stations A4 and B4 due to the influence of Mediterranean water
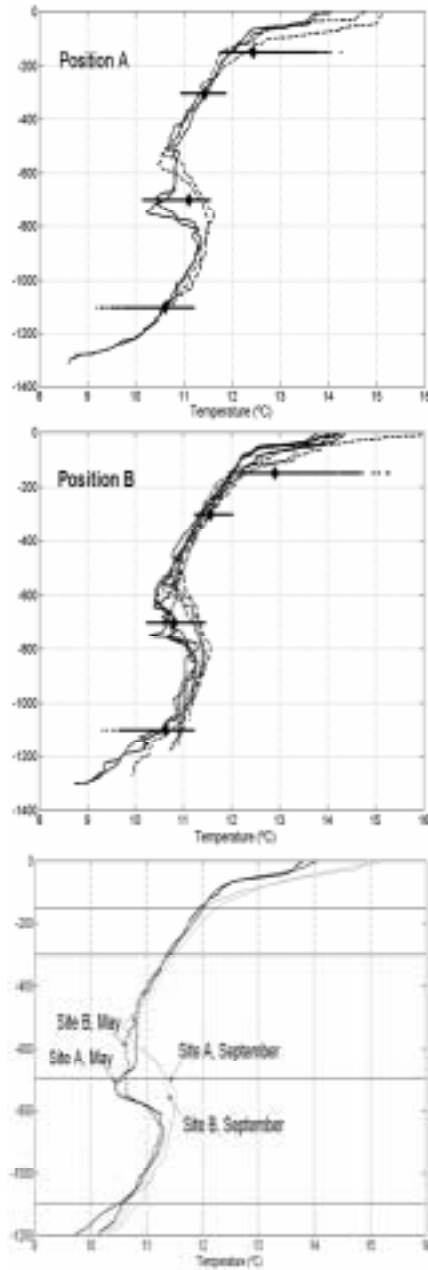
Figure 5.- Upper panel: Temperature profile at stations 6 and 7 (see Figure 1) nearby position A in May (full line) and in September (dotted line). Centre panel: Temperature profiles at stations 22, 23, 24 and 35 (see Figure 1) nearby position B in May (full line) and in September (dotted line). Dots located at the depths of the instruments are the observed temperature at each depth. Bottom panel: horizontally averaged and vertically smoothed temperature profile nearby positions A and B in May and September (see legend). Horizontal lines in this panel indicate the depth of the instruments. Vertical axis is depth in metres.
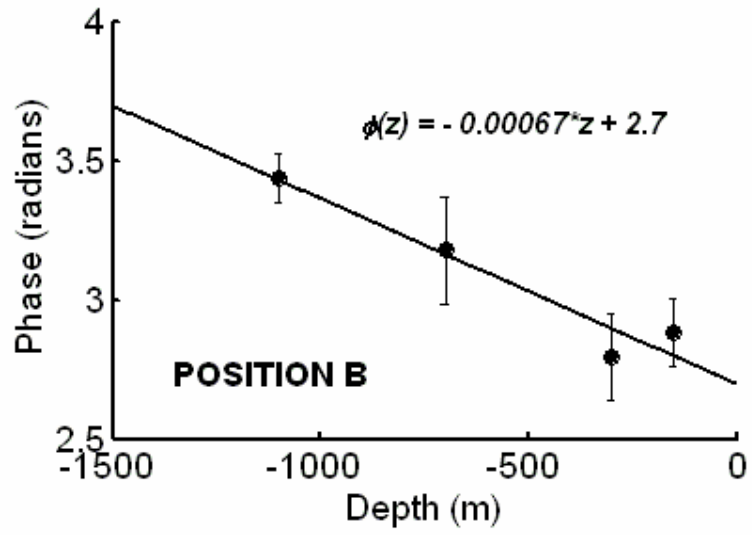
Figure 6.- Linear fit of phase of stations in position B with depth. Dots are the computed phases and bars indicates the error (see Table 4). The slope is negative.
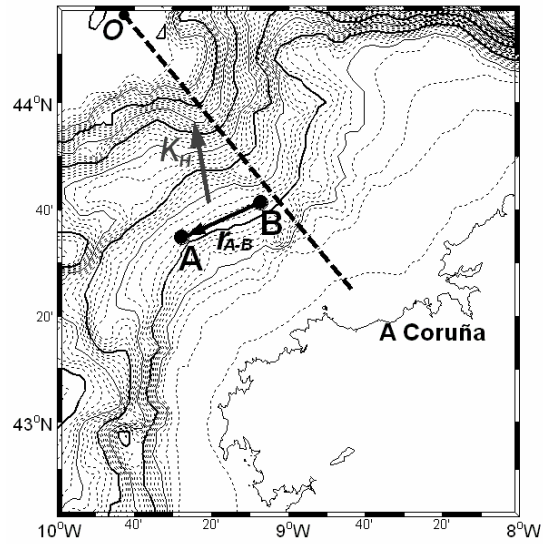
Figure 7.- Map of the area showing the bathymetry (successive isolines are separated 100m; solid lines are 500, 1500, 2500, 3500 and 4500m, thick solid lines are 1000, 2000, 3000, 4000 and 5000m). Vectors r_{A-B} and k_H mentioned in the text have been plotted. The phase lag between stations B4 and A4, which depends on the relative orientation of these vectors, is 19° in case that k_H is oriented along the thick dashed line (see text for details). Letter "O" in the upper left corner indicates the origin of distances in Figure 8.
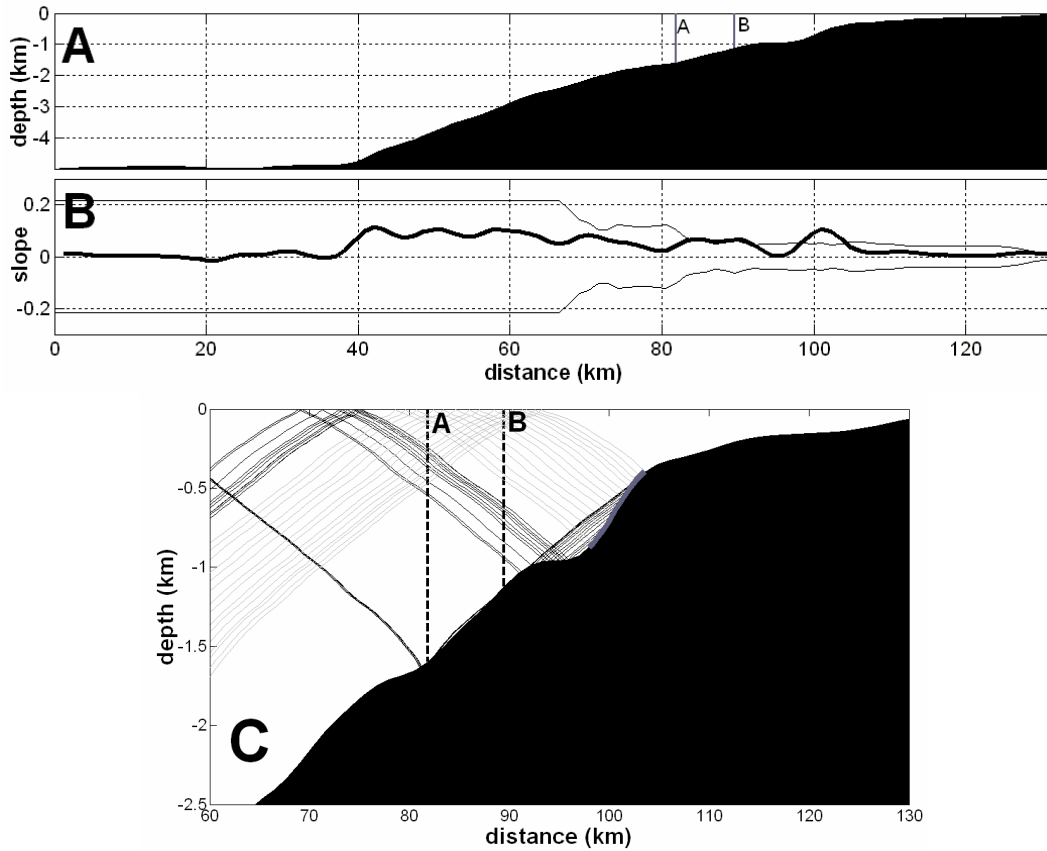
Figure 8.- A) Bottom profile along the transect marked by the dashed line in Figure 7. The origin of distances along the *x*-axis has been arbitrarily chosen in point "O" in that Figure. The vertical lines indicate the projection of positions A and B on the selected transect. B) Slope of the sea floor along the profile shown in A (thick line) and slope of the characteristics computed from equation 7 using the buoyancy frequency deduced from the CTD stations (thin line). The vertical profile of N^2 seawards of the outermost station, where data are not available, has been considered the same as the profile of the outermost station (see text for details). The bottom slope is supercritical wherever the thick line is above the thin line. It is clearly supercritical around $x = 100$ km and nearly critical between $x = 80$ and $x = 90$ km. C) Path of the internal tide beams after being reflected seawards by the supercritical continental slope. The supercritical portion of the slope is indicated by the thick grey line.
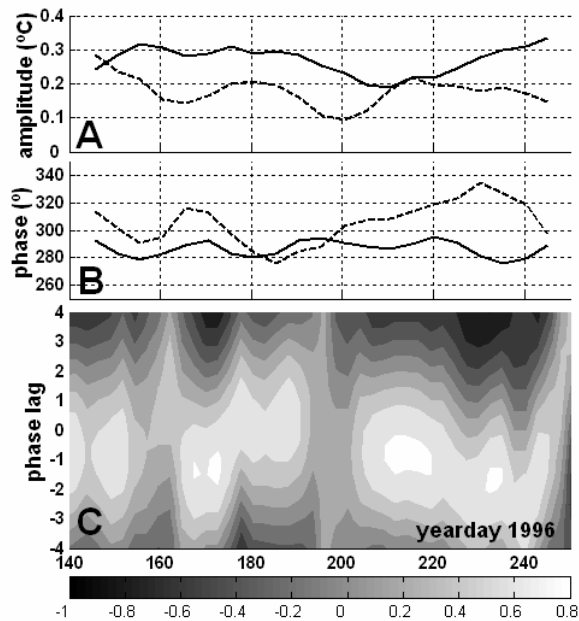
Figure 9.- A) Amplitude of the M2 temperature signal in A4 (dashed line) and B4 (solid line) computed sequentially for pieces 20-day long. This length separates constituents M2 and S2 and therefore the amplitudes are not affected by the fortnightly modulation of the spring-neap cycle. The *x*-axis indicates the central day of the piece. B) Same as A for phases. C) Contours of the correlation coefficient between temperatures in A4 and B4 as a function of time (*x*-axis) and phase-lag (*y*-axis). The correlation has been calculated over pieces 7-day long in order to have better time resolution.
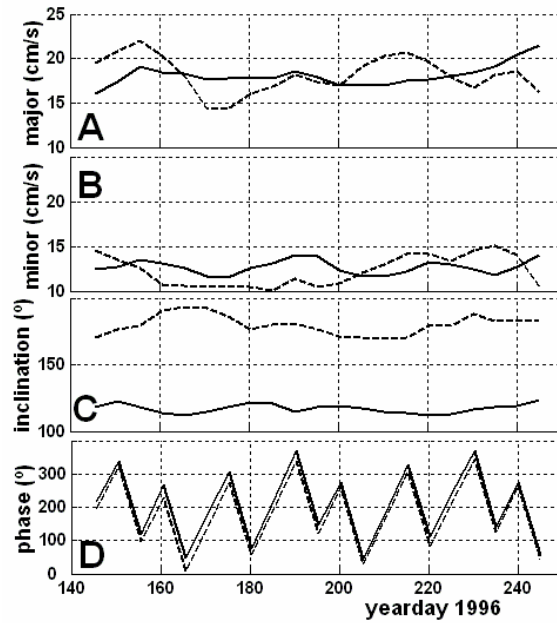
Figure 10.- A) Amplitude of the major semiaxis of tidal ellipse in A4 (dashed line) and B4 (solid line) computed sequentially for pieces 20-day long. This length separates constituents M2 and S2 and therefore the amplitudes are not affected by the fortnightly modulation of the spring-neap cycle. The *x*-axis indicates the central day of the piece. Panels B), C) and D) are same as A for minor semiaxis, inclination of the ellipse and phase lag.